Over-the-Barrier Transition State Analogues and Crystal Structure with *Mycobacterium tuberculosis* Purine Nucleoside Phosphorylase[†,‡]

Andrzej Lewandowicz,[§] Wuxian Shi,[§] Gary B. Evans,[||] Peter C. Tyler,[||] Richard H. Furneaux,[||] Luiz A. Basso,[⊥] Diogenes S. Santos,[⊥] Steven C. Almo,[§] and Vern L. Schramm*[,§]

Department of Biochemistry, Albert Einstein College of Medicine, 1300 Morris Park Avenue, Bronx, New York 10461, Carbohydrate Chemistry Team, Industrial Research Limited, Lower Hutt, New Zealand, and Departamento de Biologia Molecular e Biotecnologia, Universidade Federal do Rio Grande do Sul, Avenida Bento Goncalvesc 9500, Porto Alegre-RS 91501-790, Brazil

Received March 7, 2003

ABSTRACT: Stable chemical analogues of enzymatic transition states are imperfect mimics since they lack the partial bond character of the transition state. We synthesized structural variants of the Immucillins as transition state analogues for purine nucleoside phosphorylase and characterized them with the enzyme from *Mycobacterium tuberculosis* (MtPNP). PNPs form transition states with ribooxacarbenium ion character and catalyze nucleophilic displacement reactions by migration of the cationic ribooxacarbenium carbon between the enzymatically immobilized purine and phosphate nucleophiles. As bond-breaking progresses, carbocation character builds on the ribosyl group, the distance between the purine and the carbocation increases, and the distance between carbocation and phosphate anion decreases. Transition state analogues were produced with carbocation character and increased distance between the ribooxacarbenium ion and the purine mimics by incorporating a methylene bridge between these groups. Immucillin-H (ImmH), DADMe-ImmH, and DADMe-ImmG mimic the transition state of MtPNP and are slow-onset, tight-binding inhibitors of MtPNP with equilibrium dissociation constants of 650, 42, and 24 pM. Crystal structures of MtPNP complexes with ImmH and DADMe-ImmH reveal an ion-pair between the inhibitor cation and the nucleophilic phosphoryl anion. The stronger ion-pair (2.7 Å) is found with DADMe-ImmH. The position of bound ImmH resembles the substrate side of the transition state barrier, and DADMe-ImmH more closely resembles the product side of the barrier. The ability to probe both substrate and product sides of the transition state barrier provides expanded opportunities to explore transition state analogue design in *N*-ribosyltransferases. This approach has resulted in the highest affinity transition state analogues known for MtPNP.

The large rate enhancements imposed by enzymatic reactions occur by lowering the transition state barrier. Achieving the transition state is typically 10^{10} to 10^{15} more probable on the enzyme than in uncatalyzed reactions, and rate enhancements of 10^{23} have been reported (*1*). Stable mimics of the substrate molecule at the transition state trap this energy of catalysis as stable binding energy and therefore have the potential to bind 10^{10} to 10^{23} times more tightly than reactant molecules (*2*−*4*). The tight binding of transition state analogues is a thermodynamic phenomenon and is independent of the dynamic motions that may be involved in achievement of the transition state. Thus, knowledge of enzymatic transition states has been a long-sought goal. The application of multiple kinetic isotope effects provides a bond order and geometrical solution to enzymatic transition states in favorable cases (*5*−*7*). From this analysis, quantum chemistry approaches provide a molecular electrostatic potential surface comparison of the substrate, transition state, and products of the reaction (*8*). These structures provide a blueprint for the design of inhibitors more closely resembling the transition state than the reactant states (*9*−*11*). Here, we explore the effects of altered transition state analogue charge and geometry by increasing the distance between the groups used to mimic the purine leaving group and the ribooxacarbenium ion that characterizes the transition state (Figure 1). These analogues are characterized with the homotrimeric PNP from *Mycobacterium tuberculosis* by both kinetic analysis and X-ray crystallography.

Bovine purine nucleoside phosphorylase is the prototype of the homotrimeric PNPs, and the transition state structure of bovine PNP[1] has been solved for the arsenolysis of inosine (*12*, *13*). It provides the only transition state information presently available for any PNP. The transition state is reached with 0.36 Pauling bond order remaining in the *N*-ribosidic bond, but only 0.03 bond order to the attacking phosphate, corresponding to nuclear separations of 1.77 and 3.0 Å, respectively (ref *13*; Figure 1). This degree of

[†] This work was supported by research grants from the National Institutes of Health, the New Zealand Foundation for Research, Science and Technology, and the CNPq/MCT (Millennium Project) of Brazil.

* Corresponding author. Telephone: (718) 430-2813. Fax: (718) 430-8565. E-mail: vern@aecom.yu.edu.

[‡] The X-ray coordinates have been submitted to the Protein Data Base, ID code 1N3I.

[§] Albert Einstein College of Medicine.

[||] Industrial Research Limited.

[⊥] Universidade Federal do Rio Grande do Sul.

10.1021/bi0343830 CCC: $25.00
Published on Web 05/03/2003

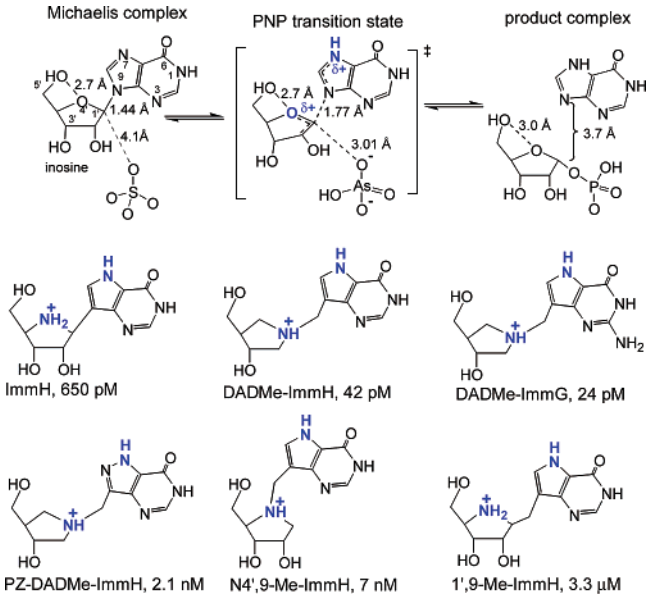

FIGURE 1: Phosphorolysis of inosine catalyzed by PNP with features of the transition state and selected features for Michaelis complexes. The complexes of bovine PNP with inosine and sulfate or hypoxanthine and ribose 1-phosphate reveal the distances between atoms as shown. At the transition state, distances shown are from KIE studies (*12*, *13*). Structures of inhibitors with features related to the transition state are indicated with their abbreviated names and K_i* values. Atomic numbering is shown for inosine. For consistency, this numbering system is used for all inhibitors but is inconsistent with IUPAC nomenclature.

N-riboside bond order at the transition state is unusual for *N*-ribosyltransferases since purine nucleoside and nucleotide hydrolases as well as ADP-ribosyltransferases and oligonucleotide purine *N*-ribohydrolases all reveal lower *N*-ribosyl bond order at their transition states (*14*). This early transition state for bovine PNP is the result of strong leaving group forces to the purine group (*15*). Immucillin-H was designed to match the transition state for bovine PNP and is a 23 pM inhibitor for its cognate enzyme. It is a weaker inhibitor for PNPs from other species, possibly because the covalent C−C ribosidic bond is a better mimic of the early transition state known to characterize the bovine enzyme. Here, we explore the interaction of MtPNP with unique transition state analogues synthesized to vary the distance between the cationic oxacarbenium ion mimic and the purine leaving group.

While many bacterial PNPs are hexameric, that from MtPNP is trimeric and closely resembles human and bovine PNPs in protein architecture and catalytic site contacts (*16*). However, Immucillin-H binds less tightly to MtPNP than to bovine PNP, suggesting that MtPNP has a transition state poise different from that of bovine PNP (*14*).

[1] Abbreviations: ImmH, Immucillin-H, (1*S*)-1-(9-deazahypoxanthin-9-yl)-1,4-dideoxy-1,4-imino-D-ribitol; DADMe-ImmH, 4′-deaza-1′-aza-2′-deoxy-1′-(9-methylene)-Immucillin-H, (3*R*,4*R*)-*N*-[(9-deazahypoxanthin-9-yl)methyl]-4-hydroxymethyl-pyrrolidin-3-ol; 1′,9-Me-ImmH, 1′-(9-methylene)-Immucillin-H, 1′-[(9-deazahypoxanthin-9-yl)methyl-1,4-dideoxy-1,4-imino-D-ribitol; DADMe-ImmG, (3*R*,4*R*)-1-[(9-deazaguanin-9-yl)methyl]-4-hydroxymethyl-pyrrolidin-3-ol; PZ-DADMe-ImmH, (3*R*,4*R*)-*N*-[(8-aza-9-deazahypoxanthin-9-yl)methyl]-4-hydroxymethyl-pyrrolidin-3-ol; N4′,9-Me-ImmH, 1,4-dideoxy-1,4-imino-*N*-(3*H*,5*H*-pyrrolo[3,2-*d*]pyrimidin-4-one-7-yl)methyl]-D-ribitol; PNP, purine nucleoside phosphorylase; MtPNP, purine nucleoside phosphorylase from *Mycobacterium tuberculosis*.

An inherent difficulty in the design of transition state analogues is the stable covalent nature of transition state analogues, while the transition state structure has partly dissociated, nonequilibrium bond lengths with partial charges. Transition state analogues can be either slightly smaller or larger but never exactly equal in size or charge to the actual transition state. Likewise, they can be neutral or designed to carry unit charge but not the partial charges of the transition state. Here, we evaluate several sizes and charge distributions in transition state analogues of MtPNP by kinetic and structural methods. We use a distinct molecular scaffold to produce DADMe-Immucillins and compare them to ImmH (Figure 1). These transition state analogues have shifted the location of the cationic charge to the position of the carbocation that is known to develop at the transition state. The inhibitors have a higher affinity for MtPNP than any inhibitors described previously. X-ray structure reveals that their increased affinity results from more favorable ion-pair formation between the cationic mimic of the oxacarbenium ion and the anionic phosphate nucleophile.

MATERIALS AND METHODS

Synthesis of DADMe-Immucillin-H and 1′-(9-Methylene)-Immucillin-H. Synthesis of DADMe-Immucillin-H was achieved via the reductive amination of 5-*N*-benzyloxymethyl-4-methoxy-3*H*,5*H*-pyrrolo[3,2-*d*]pyrimidine-7-carbaldehyde, derived from the lithiation and subsequent formylation of the previously reported 5-*N*-benzyloxymethyl-7-bromo-4-methoxy-3*H*,5*H*-pyrrolo[3,2-*d*]pyrimidine (*17*) with (3*R*,4*R*)-3-hydroxy-4-hydroxymethylpyrrolidine (*18*). Acid deprotection of the product followed by chromatographic purification afforded DADMe-Imm-H as the HCl-salt that was characterized by NMR, mass spectroscopy, and elemental analysis. 1′,9-Me-ImmH was prepared via the addition of lithiated *tert*-butyl acetate to the previously reported imine, 5-*O*-*tert*-butyldimethylsilyl-1,*N*-dehydro-1,4-dideoxy-1,4-imino-2,3-*O*-isopropylidine-D-ribitol (*19*). The *tert*-butyl acetate moiety was converted to a propionitrile residue that was elaborated to the corresponding pyrrolopyrimidine using a standard method (*20*). Acid deprotection followed by chromatographic purification afforded 1′,9-Me-ImmH as the HCl salt that was characterized by NMR, mass spectoscopy, and elemental analysis. The purified 1′,9-Me-ImmH and DADMe-ImmH were >95% purity and were stored as dried HCl-salts until use. The extinction coefficient of solutions was assumed to be equivalent to that of 9-deazainosine; 9.54 mM^{-1} cm^{-1} at 261 nm (*21*). The full description of the chemical synthesis of DADMe-ImmH and related analogues will be published elsewhere.

Protein Preparation. PNP from *M. tuberculosis* was cloned and expressed in *Escherichia coli* and purified as described earlier (*22*). Briefly, MtPNP was produced in *E. coli* BL21(DE3) cells bearing a pET-23(+)::deoD plasmid. Preparations used for both kinetic analysis and for X-ray crystallography were >95% homogeneous by denaturing gel electrophoresis.

Determination of Kinetic and Inhibition Constants. Continuous assays for MtPNP coupled the production of hypoxanthine to uric acid by xanthine oxidase (*23*). MtPNP (2.7 nM) was added to inosine (1 mM) and xanthine oxidase (60 mU/mL) in 50 mM KPO_4 buffer pH 7.4 (25 °C). The

increase in absorbance was monitored at 293 nm ($\epsilon_{293} = 12.9$ mM^{-1}). For K_i and K_i* analysis, the amounts of enzyme and inhibitor were adjusted to give an absorbance change <1.0 for the full analysis, corresponding to less than 7.8% conversion of substrate to product and limiting ribose 1-phosphate formation to less than 78 μM. Coupling with xanthine oxidase prevents hypoxanthine accumulation and approach to thermodynamic equilibrium. Initial inhibition (K_i) was determined by fitting to the equation for competitive inhibition, $v_i = (k_{cat}S)/(K_m(1+ I/K_i) + S)$, where v_i, k_{cat}, K_m, K_i, and I are initial rates, catalytic turnover number, Michaelis constant, inhibitor dissociation constant, and free inhibitor concentration, respectively. The substrate concentration (S) of 1 mM exceeds the K_m (23 μM) by a factor of 44 and increases the amount of inhibitor (I) that can be added to permit I > E concentrations. Under most conditions, the concentration of I was >10 times that of enzyme as required for fitting to the equation for competitive inhibition (*24*). For powerful inhibitors where E and I are within an order of magnitude in concentration, the free inhibitor was determined by the relationship $I = I_t - (1 - v_i/v_o)E_t$, where I_t is total inhibitor concentration, v_i and v_o are inhibited and uninhibited steady-state rates, and E_t is total enzyme catalytic site concentration. This expression can be applied to the pre- or post-slow-onset inhibition phase with equal validity, provided that the steady-state conditions are well-defined. With the xanthine oxidase assay, there is a small but significant time-dependent loss of catalytic activity, so instantaneous slope measurements are required both for inhibited and for uninhibited rates under the same reaction conditions except for presence of inhibitor. The dissociation constant for the tightly bound complex (K_i*) was determined by the same equation after the slow-onset equilibrium had been achieved. Apparent values of k for DADMe-ImmH and DADMe-ImmG were obtained by fitting progress curves at each inhibitor concentration to the equation $P = v_s t + (v_o - v_s)(1 - e^{-kt})/k$ where P is product, v_s and v_o are inhibited and initial reaction rates, and t is time (*23*). Rate constants k_5 and k_6 were established from $k = k_6 + k_5(I/K_i/(1 + S/K_m + I/K_i))$ and $k_5 = k_6(K_i/K_i* - 1)$ after establishing the apparent constant k from the progress curves.

Previous studies of MtPNP and its inhibition by Immucillin-H used 7-methyl-6-thioguanosine as substrate at pH 7.6 and monitored production of the 7-methyl-6-thioguanine at 360 nm. Using that assay, K_i and K_i* values of 2.2 and 0.04 nM were reported, but reanalysis of that data indicates the correct value of K_i* to be approximately 0.6 nM (*22*). Here, we use inosine as substrate at pH 7.5, 25 °C and establish K_i and K_i* values of 6.6 and 0.65 nM (see Results and Discussion). In the present study, we use the coupled assay with inosine as substrate and report all kinetic constants of the competitive inhibitors with respect to this physiological substrate.

Enzyme−Inhibitor Dissociation Studies. Relaxation of the tightly bound complex E*I occurs via the step k_6 (Scheme 1). When $k_4 \gg k_6$ or k_5, dilution of the E*I complex in the presence of excess inosine causes activity regain with a first-order rate constant equal to k_6 (*24*). Studies of k_6 were performed with DADMe-ImmH, DADMe-ImmG, and ImmH. Samples of 51 μM MtPNP and 100 μM inhibitor (16 μL) were incubated for 5.5 h, 25 °C in 20 mM Tris-HCl pH 7.5 in the presence or absence of 65 mM phosphate. Samples were diluted 1:500 into the same buffer followed by an additional 1:100 dilution into assay mixtures as described above for a total dilution of 50 000. Assay mixtures contained 1 mM inosine, 44 × K_m to provide competition against recombination of free inhibitor. It should be noted that a 1:50 000 dilution of 100 μM inhibitor yields 2 nM inhibitor. Depending on the K_i* value, partial or complete activity is regained.

Scheme 1: Slow-Onset Inhibition for Tight-Binding Inhibitors (*24*)[a]

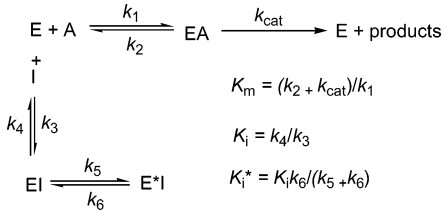

[a] For the assays seen in Figure 2, E is the MtPNP•PO_4 complex, A is inosine, and I is one of the tight-binding Immucillin inhibitors. EI is the rapidly reversible complex with inhibitor. The slow-onset, tight-binding step is k_5, forming E*I, a conformationally tightened complex that is incapable of releasing I without relaxing via k_6 to EI.

Crystal Growth, X-ray Diffraction, Data Collection, and Analysis. Crystals were grown from a solution containing a 1:1 mixture (2 μL of each) of 730 μM PNP, 1.1 mM DADMe-ImmH, 3 mM sodium phosphate pH 8.0 with the reservoir solution containing 100 mM Tris-HCl pH 8.0, 25% poly(ethylene glycol) 4000 and 25 mM $MgCl_2$ (Hampton crystallography screen). This procedure is similar to that reported earlier for crystals with ImmH except for protein concentrations and DADMe-ImmH replacing ImmH (*16*). Diffraction from the crystals was consistent with the trigonal space group ($a = b = 102.84$ Å, $c = 128.76$ Å) containing a trimer in the asymmetric unit.

Crystals were transferred to a reservoir solution containing 20% glycerol and were frozen at −178 °C. X-ray diffraction data were collected on a R-AXIS IV area detector coupled to a RIGAKU RU-H3R X-ray generator. Data were reduced using the HKL package (*25*) and were 95.8% complete to 1.9 Å resolution with R_{sym} of 3.6%. The structure was refined with CNS (*26*) using the MtPNP•ImmH•PO_4 complex as a starting model. The R_{cryst} and R_{free} were 28.6 and 29.0% following the initial round of rigid-body refinement and simulated annealing. One DADMe-ImmH and one phosphate molecule were built into the electron densities of each active site using the program O (*27*). The final model includes residues 7−268, DADMe-ImmH, a phosphate for each monomer, and 432 water molecules, to give R_{crys} and R_{free} of 18.3 and 21.3%, respectively (Table 1). Analysis by PROCHECK (*28*) indicates 91.6% of residues in the most favored conformation, 7.9% in the additionally allowed region, and only Thr209 in the disallowed region. Thr209 demonstrates good electron density in the $F_o - F_c$ omit map and is adjacent to Ser208, a phosphate binding residue. The structure has been submitted to the Protein Data Bank, PDB ID code 1N3I.

Computational Chemistry. Molecular electrostatic potential surfaces of inhibitor molecules were generated by Gaussian 98 (*29*). Structures were optimized using the PM3 semiempirical level of theory, with the geometry restrained to fit crystallographic constraints. The transition state model

Table 1: Data Collection and Refinement Statistics for *M. tuberculosis* PNP

resolution range, Å	20−1.9 (1.97−1.90)
completeness, %	95.8 (76.9)
R_{merge}, %	3.6 (10.5)
mean $I/\sigma(I)$	45.9 (10.3)
no. of reflections	
unique	59 925
total	321 763
Refinement	
R_{cryst} (%)	18.3
R_{free} (%)	21.3
no. of amino acids	786
no. of ligands	3 DADMe-ImmH 3 phosphate
no. of waters	432
ave. B factor (Å^2), protein atoms	17.8
ligands	12.6
water	21.9
RMSD, bond (Å)	0.004724
angle (deg)	1.32049

constrained the N-9 to C-1′ bond to 1.77 Å with N-7 protonated as established from KIE studies of bovine PNP (*13*). Molecular electrostatic potential surfaces were calculated in the CUBE function of Gaussian 98 and visualized by the Molekel 4.0 package (*30*).

RESULTS AND DISCUSSION

Inhibition of MtPNP. Initial rate kinetic studies with DADMe-ImmH demonstrated slow-onset, tight-binding inhibition of MtPNP (Figure 2, Table 2). The initial rate inhibition (K_i) occurs prior to slow-onset inhibition and corresponds to the dissociation constant from the initial interaction of the inhibitor. It has been proposed that K_i represents the reversible binding of the neutral form of ImmH (*22*). Similar data is not yet available for the other inhibitors of Figure 1. After the initial rate period, a first-order change occurs to a more inhibited steady-state that determines K_i* (Scheme 1; ref *24*). MtPNP is inhibited by DADMe-ImmH with K_i and K_i* values of 1.3 nM and 42 pM, respectively, indicating a 31-fold increase in affinity because of slow-onset. By comparison, ImmH (Figure 1) inhibited MtPNP with K_i and K_i* values of 6.6 and 0.65 nM, respectively (Table 2). Inhibition of MtPNP by DADMe-ImmH is of significantly higher affinity than by ImmH in both the K_i and the K_i* phases of inhibition.

Formation and release of the tightly bound MtPNP•DADMe-ImmH complex requires conformational changes defined by k_5 to form the E*I complex and k_6 to relax it (EI ↔ E*I). Analysis of the slow-onset step for DADMe-ImmH gave a k_5 value of 9.9×10^{-3} s^{-1}, and k_6 was calculated to be 3.3×10^{-4} s^{-1} by solving the equations described above for k_6. The corresponding k_6 value for ImmH is 2.4×10^{-3} s^{-1}, a factor of 7 more rapid. These rates can be experimentally confirmed by measuring the release of the inhibitors from the MtPNP•Immucillin and MtPNP•PO_4•Immucillin complexes (Figure 2, middle and lower panels). DADMe-ImmH has a higher affinity in the initial complex (1.3 vs 6.6 nM) and a slower conformational relaxation (3.3×10^{-4} s^{-1} vs 2.4×10^{-3} s^{-1}) than ImmH, both of which contribute to the decreased value for K_i*.

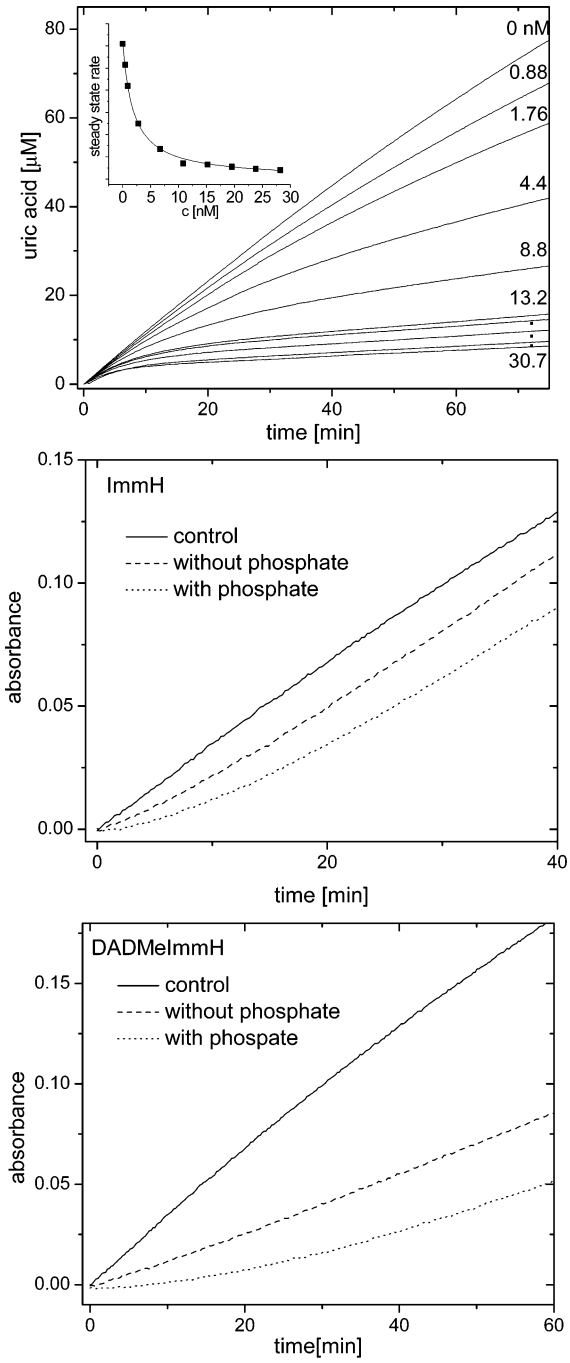

FIGURE 2: Inhibition of MtPNP. Inhibition by DADMe-ImmH is shown in the upper panel, and K_i* determination is shown in the inset. Regain of activity from PNP•ImmH•PO_4 and PNP•DADMe-ImmH•PO_4 complexes (middle and lower panels) demonstrates the greater affinity of DADMe-ImmH.

Catalytic activity regained from complexes of MtPNP•ImmH was complete by 15 min following dilution into assay mixture, while complexes of MtPNP•PO_4•ImmH required over 20 min and were more inhibited throughout the assay (Figure 2, middle panel). The initial rates on initiation of the assay represent the fraction of enzyme free and rapidly dissociable ImmH at the time the assay was initiated. The assay contains excess PO_4, causing the rapid equilibration of MtPNP•PO_4•ImmH from MtPNP•ImmH. The initial rate upon dilution suggests that 43% of MtPNP exists as MtPNP•ImmH following dilution to 100 nM enzyme and 200 nM, indicating a dissociation constant of 210 nM. Initial

Table 2: Inhibition of *Mycobacterium tuberculosis* PNP by Immucillins

inhibitor	K_i	K_i*	k_5	k_6
DADMe-Immucillin-H	1.3 ± 0.1 nM	42 ± 2 pM	9.9×10^{-3} s^{-1}	3.3×10^{-4} s^{-1}
DADMe-Immucillin-G	540 ± 40 pM	24 ± 1 pM	7.1×10^{-3}	3.3×10^{-4}
Immucillin-H	6.6 ± 1.0 nM	650 ± 20 pM	2.2×10^{-2} s^{-1}	2.4×10^{-3} s^{-1}
PZ-DADMe-Immucillin-H	2.1 ± 0.2 nM	no slow-onset	none	none
N4′,9-Me-Immucillin-H	7.0 ± 0.2 nM	no slow-onset	none	none
1′,9-Me-Immucillin-H	3.3 ± 2.2 μM	no slow-onset	none	none

Scheme 2: Binding Equilibrium for Substrates, ImmH, and DADMe-ImmH to MtPNP[a]

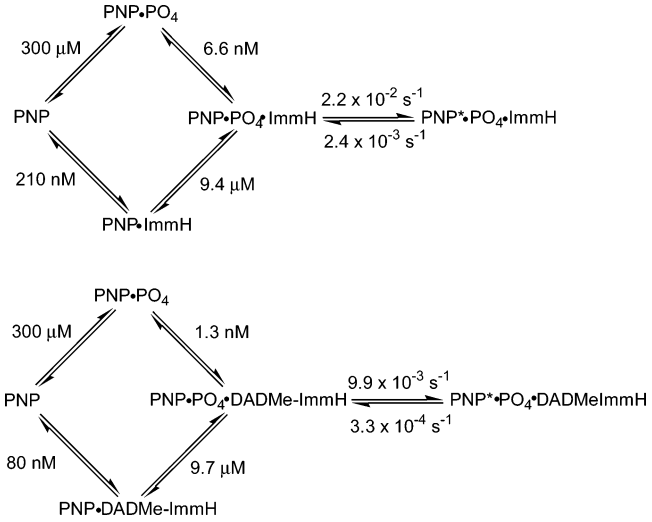

[a] The constant for phosphate is from ref *22*, and all other constants are determined as indicated in the text.

rate studies (Table 2) establish that phosphate tightens the initial complex to 6.6 nM (Scheme 2). A similar pattern is seen with DADMe-ImmH, except that incubation with DADMe-ImmH in the absence of PO_4 sequesters slightly more of the enzyme in the MtPNP•DADMe-ImmH complex for a dissociation constant of 80 nM, tightened by phosphate in the ternary MtPNP•PO_4•DADMe-ImmH complex (K_d of 1.3 nM). This complex does not completely dissociate during the 40 min assay period even in the presence of excess inosine. These estimates of dissociation constants for binary and ternary MtPNP complexes permit construction of thermodynamic equilibria for the rapidly reversible formation of the ternary complexes. The rate constants k_5 and k_6 complete the description for formation and equilibrium of the tightly bound forms following slow-onset inhibition (Scheme 2).

Guanosine nucleosides are substrates for trimeric PNPs and have similar k_{cat} but slightly lower K_m values (*31*). We synthesized DADMe-ImmG to compare its affinity with DADMe-ImmH. DADMe-ImmG is also a slow-onset inhibitor with K_i and K_i* values of 540 and 24 pM, respectively (Table 2). Conversion of the five-membered ring of the purine analogue to a pyrazolo group gives PZ-DADMe-ImmH with a decreased pK_a at N-7 (8.6 vs 10) and tautomeric equilibrium with 77% protonation N-7 (ref *31*; Figure 1). Pyrazolo substitution is unfavorable for MtPNP since the K_i increases to 2.1 nM with this substitution, and no slow onset inhibition is observed. An even greater K_i value of 7 nM is found for N4′,9-Me-ImmH, and no slow-onset is observed (Figure 1, Table 2).

Insertion of a methylene bridge between the 9-deazahypoxanthine and the iminoribitol groups of ImmH gives 1′,9-Me-ImmH, closely related to both ImmH and DADMe-ImmH (Figure 1). Inhibition of MtPNP by 1′,9-Me-ImmH gave a K_i value of 3.3 μM with no indication of slow-onset inhibition in experiments similar to Figure 2. The pK_a values of N-7 and N-4′ are unperturbed in this molecule, but the additional distance between the 9-deazahypoxanthine leaving group and the iminoribitol oxacarbenium ion mimic decreases binding affinity by a factor of 5000 relative to ImmH and 54 000 relative to DADMe-ImmH. As shown below, this loss of binding is proposed to result from misalignment of H-bonds to 9-deazahypoxanthine and/or the iminoribitol group without compensation by a strengthened ionic interaction between the bound phosphate anion and the cationic nitrogen.

Molecular Electrostatic Potential Surfaces for Inosine, ImmH, DADMe-ImmH, and 1′,9-Me-ImmH. Binding affinity for transition state analogues correlates closely with the similarity of geometry and molecular electrostatic potential surfaces to that of the actual transition state (*10*). Molecular electrostatic potential surfaces can be compared for inosine, the transition state, and the analogues described here. The geometry of substrate, transition states, and transition state analogues were fixed to that imposed by MtPNP for calculation of the electrostatic potentials, and the bond orders for the transition state were taken from bovine PNP (the only PNP transition state available; ref *13*). The partial positive charge of the transition state for PNP is centered near C-1′ on the ribosyl group, and the partial loss of C-1′, N-9 bonding electrons to the leaving group increases the pK_a at N-7 (compare inosine with inosine at the transition state in Figure 3a,b). Immucillin-H resembles the transition state more than substrate, but the cationic charge is centered on the 4′-N group rather than at C-1′, its location in the actual transition state (ref *32*; Figure 3c). The C-1′ to C-9 bond distance in ImmH is fixed at 1.5 Å because of the covalent bond, but it is 1.8 Å in the transition state. ImmH is a N-4′ cation when bound to MtPNP (*33*) giving the carbocation mimic but offset by one bond from the transition state cation. As a transition state analogue, ImmH has excess cation character but in bond geometry is more like substrate (1.44 Å) than transition state (1.8 Å) or the product separation (3.7 Å) for the C-1′ to C-9 distance. The 1′,9-Me-ImmH has increased separation between the purine and the ribosyl mimics, making the C-1′ to C-9 bond distance approximately 2.4 Å. The cation remains at the 4′ rather than the 1′ position (Figure 3d). When cationic transition state analogues are bound, close contacts between the oxacarbenium mimic and phosphate occur (*15*, *16*). The 9-deaza purine of 1′,9-Me-ImmH will be forced too far into the leaving group pocket, destroying the H-bond network to N-7, O-6, and N-1. These interactions are known to be worth 7−10 kcal/mol in binding energy (*34*). The oxacarbenium ion mimic on the molecular electrostatic surface for DADMe-ImmH is located close to that of the

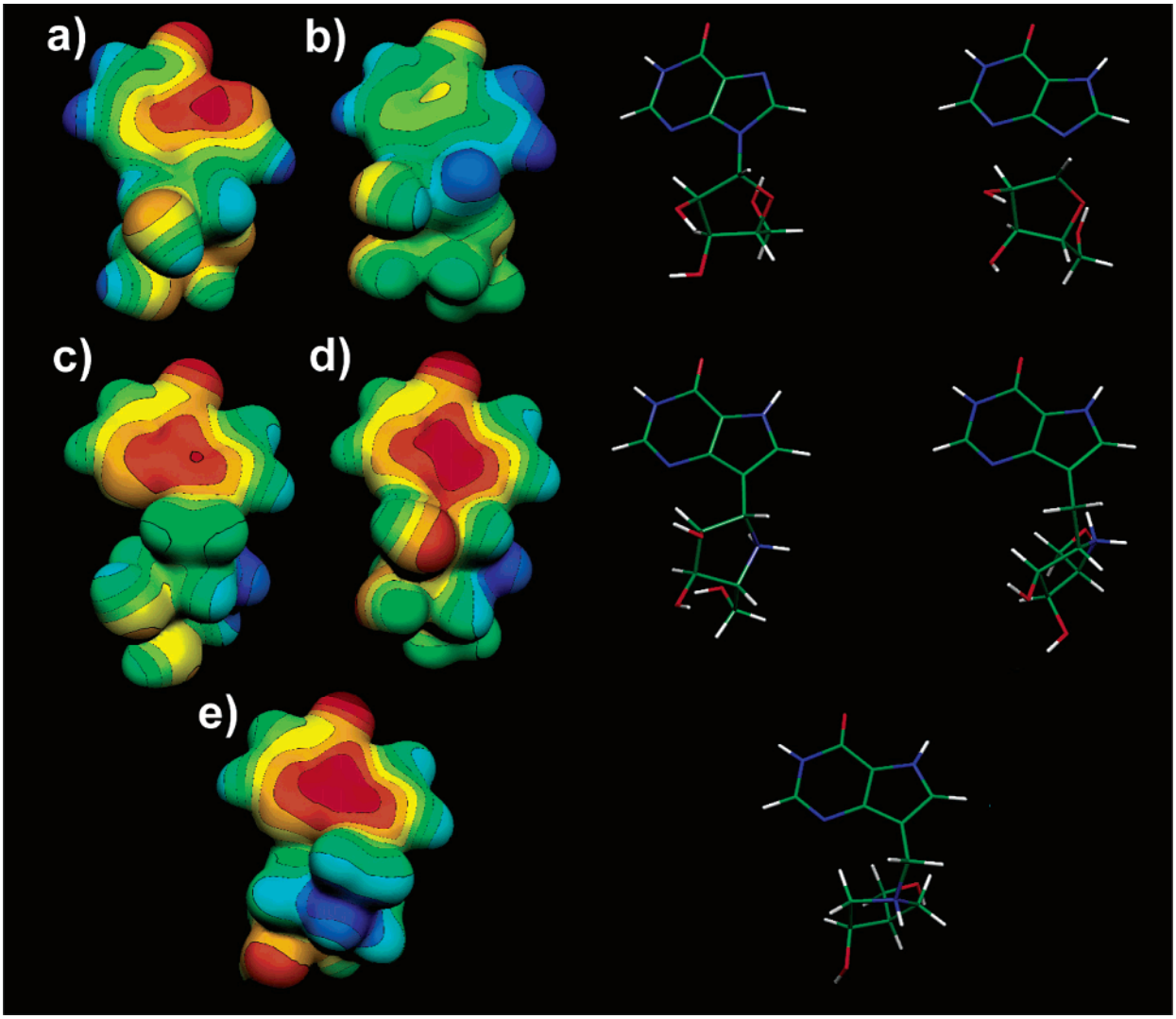

FIGURE 3: Molecular electrostatic potential surfaces for inosine (a), transition state for inosine (b), ImmH (c), 1′,9-Me-ImmH (d), and DADMe-ImmH (e). Surfaces depict the force a point charge experiences at a surface electron density of 8 mb (slightly inside the van der Waals interaction surface). Red, blue, and green represent electron-rich, electron-deficient, and neutral regions of the molecule, respectively. Structures on the right provide orientation for those on the left.

C-1′ anomeric carbon of transition state, and the elevated pK_a at N-7 is maintained to establish N-7 protonation (compare Figure 3b,e). The increased distance between the ribosyl and the purine analogues is 1.0 Å in DADMe-ImmH relative to ImmH, similar to 1′,9-Me-ImmH, and it was surprising that high affinity binding persisted. The interaction of DADMe-ImmH with MtPNP was examined by crystallography to explain the differences between ImmH and DADMe-ImmH binding.

Crystal Structure of MtPNP with DADMe-ImmH. The complex with DADMe-ImmH and phosphate was solved by molecular replacement using the previous structure of MtPNP with ImmH as the search model (*16*). The trimeric subunit structure and monomer protein folds are unchanged by the substitution of DADMe-ImmH for ImmH (Figure 4), and the backbone α-carbon atoms overlap with an RMS-deviation of 0.18 Å. The 9-deazahypoxanthine base and phosphate ion are bound in similar H-bond networks and in the same positions in the protein as is ImmH. However, the 1′-nitrogen atom of the oxacarbenium ion mimic in DADMe-ImmH is moved closer to bound phosphate (Figure 5). The nucleophilic phosphate oxygen in the complex with ImmH is 3.3 Å from the position of the anomeric carbon and 3.1 Å from the N-4′. NMR studies have established that the 4′-N of ImmH is protonated when bound to MtPNP; thus, an ion pair is formed in the complex with 3.1 Å ionic separation (*33*). Moving the nitrogen from the 4′-postion of ImmH to the 1′-position of DADMe-ImmH moves the cation to the same position as the location of the partial positive charge at the actual transition state. Computational analysis of ribooxacarbenium ions have established that the 4′-ring oxygen retains a partial negative charge while C-1′ has a partial positive charge (*32*). This permits a 2.7 Å ion-pair to form and is proposed to be responsible for the tight binding of the DADMe analogues. The presence of the methylene bridge provides a geometric change by moving deazapurine and pyrrolidine groups apart by approximately 1.0 Å relative to ImmH, forcing a closer contact between the repositioned cation and the bound phosphate. Oxygen-4 of bound phosphate is 2.7 Å from N-1′ of DADMe-ImmH, strengthening the ion-pair.

Application of Coulomb's law predicts −15.8 kcal/mol increased binding energy for this distance (point charge interactions in a vacuum, dielectric = 1), although a medium

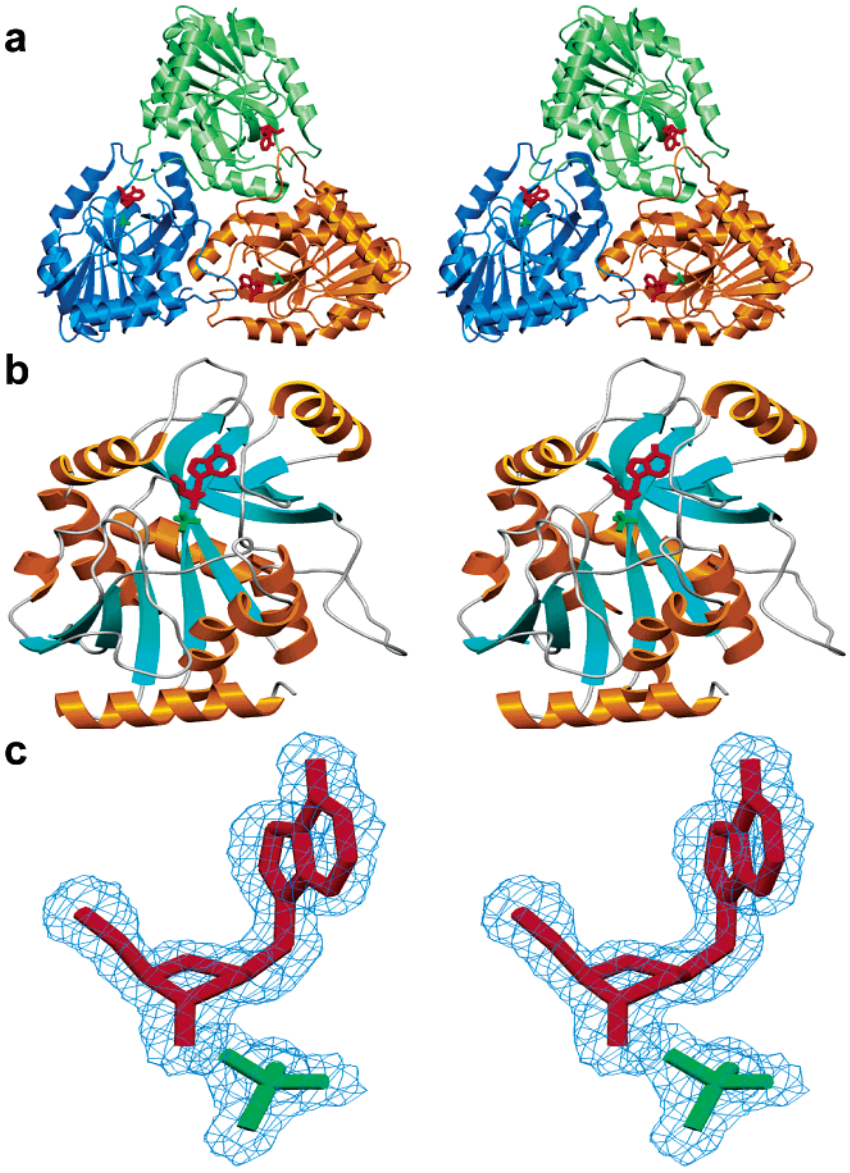

FIGURE 4: Stereoview structures of the trimer (a), monomer (b), and $F_o - F_c$ of DADMe-ImmH (c) from the complex of *M. tuberculosis* PNP•DADMe-ImmH•PO_4. DADMe-ImmH is in red, and phosphate is in green in each panel.

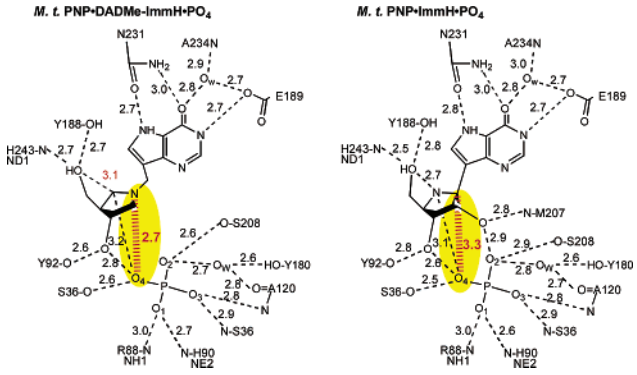

FIGURE 5: Catalytic site distances for *M. tuberculosis* PNP with ImmH or DADMe-ImmH and PO_4 in the catalytic sites. The structure with ImmH is from Shi et al. (*16*) and is included to permit comparison with DADMe-ImmH.

of increased dielectric constant reduces the energy proportionally. DADMe-ImmH lacks the 2′-OH of ImmH and therefore has fewer hydrogen-bond interactions to MtPNP. Contacts in the complex of MtPNP•ImmH•PO_4 include 13 hydrogen bonds of 2.9 Å or less, excluding the ionic interaction between the phosphate and the imino group. For the complex with DADMe-ImmH, the same analysis reveals the loss of three of these H-bonds (Figure 5). However, the more favorable ionic interaction with DADMe-ImmH compensates for the loss of H-bonds at the 2′-hydroxyl of ImmH and provides additional binding energy to alter the K_i* from 650 to 42 pM. Assuming the dielectric constant of the closed catalytic site to be near 2, the enhanced ionic interaction still provides −7.9 kcal/mol, more than sufficient to compensate for the loss of the H-bonds.

A second difference in comparing MtPNP structures with ImmH and DADMe-ImmH is the 3.1 Å distance from O-5′ to C-4′ in the complex with DADMe-ImmH. PNP has been proposed to initiate ribooxacarbenium ion formation by neighboring group interactions from the O-5′ 2.7 Å above and the O-4 of phosphate 3.1 Å below the 4′-O (ref *15;* Figure 5). Immucillin-H in the crystal is bound as the N-4′ cation, attracting O-5′ (*33*). DADMe-ImmH has a carbon at this position, and the 5′-hydroxyl relaxes to 3.1 Å from this site, within experimental error of the 3.0 Å distance found in the product complex of hypoxanthine and ribose 1-PO_4

(*15*, *35*). Despite the altered position of the 5′-hydroxymethyl group, the hydrogen bonds between the 5′-hydroxyls of both ImmH and DADMe-ImmH and His243 and Tyr188 remain within crystallographic error.

Transition State Mimics and the Reaction Coordinate of PNPs. Each of the tight-binding Immucillins have the cationic electrostatic potential that characterizes the transition state and the reacting atoms after they pass the transition state barrier. *N*-Ribosyltransferases catalyze nucleophilic displacements by electrophile migration (*16*). At the transition state for PNPs, only a fraction of the ribooxacarbenium ion charge is formed because of residual bond order to the leaving group (*13*). After passing the barrier, full oxacarbenium character develops on the energetically favorable path to bound products. Here, we compare the distances between attacking nucleophile, anomeric carbon of the substrate or substrate analogue, transition state, and transition state analogues through the reaction coordinate of PNP. This comparison requires a composite of information from the homotrimeric PNPs. Substrate and product analogue complexes use structures of the bovine PNP from the Ealick lab since these are the highest resolution structures available for these complexes (*35*). The only experimental transition state information based on kinetic isotope effects is also from the bovine enzyme, so these three structures are directly comparable. The only PNP with crystal structures of both ImmH and DADMe-ImmH is MtPNP. Thus, these two structures are also directly comparable, and the K_i* values reported here are from these same complexes. Both bovine and MtPNPs have been solved with ImmH and PO_4 bound and permit direct comparison of the catalytic site architecture. The structures have been solved to 1.5 and 1.9 Å, respectively, and estimated coordinate errors are less than ±0.2 Å. For covalent bonds, there is no significant error in bond length on our present scale of comparisons.

Comparison of the distances between ImmH and PO_4 and catalytic site contacts in MtPNP and bovine PNP have been reported (*16*). Of the 24 contacts that characterize these interactions, 20 are within the ±0.2 Å limit as shown in Table 3. Exceptions include His243 to 5′-O, 0.4 Å shorter in MtPNPs; phosphate oxygen O_4 to N-4′, 0.3 Å longer in MtPNP; Ser208 to phosphate oxygen O_2, 0.3 Å longer in MtPNP; and the Tyr188 to 5′-O is a 2.8 Å interaction in MtPNP that is not present in bovine PNP. Thus, the catalytic site contacts are closely related and permit the distance comparisons within the indicated error limits.

Our structural mimic of the Michaelis complex is bovine PNP•inosine•SO_4 in which the nucleophilic oxygen is 4.1 Å from the C-1′, to give approximately 5.6 ± 0.2 Å in the reaction coordinate (the distance from O of the nucleophile to N9 of the leaving group purine, Figure 6; refs *16* and *35*). Reaction coordinate motion in the PNP reaction involves migration of C-1′ from the purine toward the phosphate while the purine and phosphate remain stationary (*16*). The product complex with hypoxanthine and ribose 1-phosphate indicates 3.8 Å between the 1′-C and N-9 of the hypoxanthine, with an additional 1.5 Å to the 1′-phosphoryl bridge oxygen for the reaction coordinate distance of 5.3 ± 0.2 Å, within experimental error of the reaction coordinate distance in the Michaelis complex. Bond lengths in the transition state are established directly from kinetic isotope effects, and these limits of uncertainty are approximately ±0.1 Å (*13*). The

Table 3: Catalytic Site Distances Comparing PNP from Bovine and *Mycobacterium tuberculosis*

ligand contacts (MtPNP) atom 1 to atom 2	bovine PNP•ImmH•PO_4 (Å)	MtPNP•ImmH•PO_4 (Å)
E189 to N1	2.9	2.7
E189 to O_w	2.6	2.7
O_w to O6	2.8	2.8
A234[a] to O_w	3.0	3.0
N231 to O6	3.1	3.0
N231 to N7	2.8	2.8
Y188 to O5′		2.8
H243 to O5′	2.9	2.5
O5′ to N4′	2.7	2.7
Y92 to O3′	2.8	2.8
O3′ to O4 (PO_4)	2.7	2.6
S36 to O4 (PO_4)	2.6	2.5
N4′ to O4 (PO_4)	2.8	3.1
C1′ to O4 (PO_4)	3.2	3.3
O2′ to O2 (PO_4)	2.9	2.9
M207 to O2′	2.8	2.8
S208 to O2 (PO_4)	2.9	2.9
O_w to O2 (PO_4)	2.8	2.8
Y180 to O_w	2.6	2.6
A120 to O_w	2.7	2.7
A120 to O3 (PO_4)	2.8	2.8
S36 to O3 (PO_4)	3.0	2.9
H90 to O1 (PO_4)	2.8	2.6
R88 to O1 (PO_4)	3.0	3.0

[a] MtPNP has one water intervening between O6 and A234; bovine PNP has two waters.

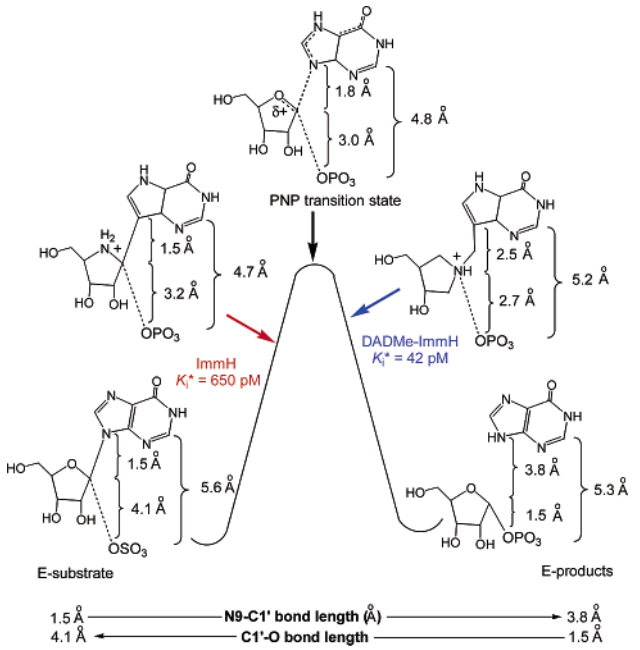

FIGURE 6: Reaction coordinate diagram for PNP based on the transition state structure. The distances for substrate and product complexes are from crystal structures of bovine PNP (*32*). The transition state structure was established from kinetic isotope effect analysis using the bovine enzyme (*12*, *13*). The structure with ImmH is for MtPNP (*24*), and the structure with DADMe-ImmH is from this paper.

C-1′ to N-9 bond at the transition state is 1.8 Å, with the nucleophile 3.0 Å below to give a reaction coordinate distance of 4.8 ± 0.1 Å, significantly compressed relative to substrate or product Michaelis complexes.

We now analyze catalytic site interactions for ImmH and DADMe-ImmH to determine if these are substrate-like or

product-like transition state mimics. ImmH bound to PNP is substrate-like in the 1.5 Å covalent bond between C-1′ and C-9 because of the phosphate anionic oxygen 3.2 Å from C-1′. Its transition state character comes from the cation at the 4′-N (*33*). The reaction coordinate distance (phosphate-O to C-9) is 4.7 ± 0.2 Å, within experimental error of the distance for the actual transition state. However, the short bond to the leaving group and the long bond to the nucleophile clearly places this structure on the substrate side of the transition state barrier in geometry, with the charge providing transition state character (Figure 6). Chemical structures of DADMe-Immucillins are also reminiscent of bi-product complexes, known to inhibit some enzymes. However, the lack of phosphate in these inhibitors and the presence of cationic charge distinguish them from true bi-product analogues.

The methylene bridge of DADMe-ImmH increases the linear distance between N-1′ and C-9 to 2.5 Å, well beyond the transition state distance of 1.8 Å for their atomic counterparts. However, the phosphate oxygen nucleophile is now only 2.7 Å from N-1′, significantly closer than it is at the actual transition state or in complexes with ImmH. This distance corresponds to a point on the reaction coordinate following transition state formation. The fully developed cation also resembles the product side of the transition state barrier since charge on the oxacarbenium continues to increase until the ribosyl group passes the midpoint of its excursion and begins to form a covalent interaction with phosphate (*15*). The crystallographic reaction coordinate distance with MtPNP•DADMe-ImmH•PO_4 is 5.2 ± 0.2 Å, within experimental error of the product complex at 5.3 ± 0.2 Å. It must be emphasized that the electrostatic features are essential for all tight-binding transition state analogues of PNP. Altering the pK_a of N-7 to make it a H-bond acceptor rather than a H-bond donor in the ImmH analogue, 3-deaza-4-aza-ImmH, reduces binding affinity by a factor of 20 million (*34*). Likewise, loss of the cationic 4′-imino group (as in 9-deazainosine) decreases affinity by a factor of 10^5 (*34*). The N-1′ cationic geometry of DADMe-ImmH is also essential to form the ion-pair with phosphate and cause tight binding. Hence, both N4′,9-Me-ImmH and 1′,9-Me-ImmH move the cation away from the phosphate anion and tight-binding is lost. Altering the location of this charge prevents simultaneous formation of the ion-pair to the phosphate as well as the crucial H-bond interactions to N-7 and O6 that are also necessary to mimic the transition state.

Other Late Transition State Inhibitors. The extensive inhibitor design programs for the human immunodeficiency virus aspartic acid protease have yielded inhibitors that can be considered analogues of catalytic events late in the reaction coordinate (*36*, *37*). However, these reactions are complicated by two transition states surrounding an unstable intermediate. There are no accurate structural models from transition state analysis to pinpoint if these inhibitors are better mimics of the transition state, reaction intermediate, or tetrahedral collected product (*37*).

Conclusions. This report establishes that different chemistries can be used to access both early and late features of an enzymatic transition state. Either side of the transition state barrier can be targeted and are both useful in the design of transition state analogues. The significance of this knowledge is that relatives of both early and late transition state analogues can now be explored in attempts to ascend higher on the slopes toward the transition state. The over-the-barrier transition state analogues described here are the most powerful inhibitors described for MtPNP.

REFERENCES

1. Miller, B. G., and Wolfenden, R. (2002) *Annu. Rev. Biochem. 71*, 847−885.
2. Wolfenden, R. (1999) *Bioorg. Med. Chem. 7*, 647−652.
3. Wolfenden, R., and Kati, W. M. (1991) *Acc. Chem. Res. 24*, 209−215.
4. Schramm, V. L. (1998) *Annu. Rev. Biochem. 67*, 693−720.
5. Cleland, W. W. (1995) *Methods Enzymol. 249*, 341−373.
6. Northrop, D. B. (2001) *Methods 24*, 117−124.
7. Schramm, V. L. (1999) *Methods Enzymol. 308*, 301−355.
8. Horenstein, B. A., and Schramm, V. L. (1993) *Biochemistry 32*, 7089−7097.
9. Bagdassarian, C. K., Brauheim, B. B., Schramm, V. L., and Schwartz, S. D. (1996) *Int. J. Quantum Chem. 60*, 73−80.
10. Bagdassarian, C. K., Schramm, V. L., and Schwartz, S. D. (1996) *J. Am. Chem. Soc. 118*, 8825−8836.
11. Braunheim, B. B., Miles, R. W., Schramm, V. L., and Schwartz, S. D. (1999) *Biochemistry 38*, 16076−16083.
12. Kline, P. C., and Schramm, V. L. (1993) *Biochemistry 32*, 13212−13219.
13. Kline, P. C., and Schramm, V. L. (1995) *Biochemistry 34*, 1153−1162.
14. Schramm, V. L. (2003) *Acc. Chem. Res.*, in press.
15. Fedorov, A., Shi, W., Kicska, G., Fedorov, E., Tyler, P. C., Furneaux, R. H., Hanson, J. C., Gainsford, G. J., Larese, J. Z., Schramm, V. L., and Almo, S. C. (2001) *Biochemistry 40*, 853−860.
16. Shi, W., Basso, L. A., Santos, D. S., Furneaux, R. H., Tyler, P. C., Blanchard, J. H., Almo, S. C., and Schramm, V. L. (2001) *Biochemistry 40*, 8204−8215.
17. Evans, G. B., Furneaux, R. H., Hutchison, T. L., Kezar, H. S., Morris, P. E., Jr., Schramm, V. L., and Tyler, P. C. (2001) *J. Org. Chem. 66*, 5723−5730.
18. Filichev, V. V., Brandt, M., and Pedersen, E. B. (2001) *Carbohydr. Res. 333*, 115−122.
19. Furneaux, R. H., Limberg, G., Tyler, P. C., and Schramm, V. L. (1997) *Tetrahedron 53*, 2915−2930.
20. Evans, G. B., Furneaux, R. H., Gainsford, G. J., Schramm, V. L., and Tyler, P. C. (2000) *Tetrahedron 56*, 3053−3062.
21. Lim, M.-I., Ren, W.-Y., Otter, B. A., and Klein, R. S. (1983) *J. Org. Chem. 48*, 780−788.
22. Basso, L. A., Santos, D. S., Shi, W., Furneaux, R. H., Tyler, P. C., Schramm, V. L., and Blanchard, J. H. (2001) *Biochemistry 40*, 8196−8203.
23. Miles, R. W., Tyler, P. C., Furneaux, R. H., Bagdassarian, C. K., and Schramm, V. L. (1998) *Biochemistry 37*, 8615−8621.
24. Morrison, J. F., and Walsh, C. T. (1988) *Adv. Enzymol. Relat. Areas Mol. Biol. 61*, 201−301.
25. Otwinowski, Z., and Minor, W. (1997) *Methods Enzymol. 276*, 307−326.
26. Brunger, A. T., Adams, P. D., Clore, G. M., DeLano, W. L., Gros, P., Grosse-Kunstleve, R. W., Jiang, J. S., Kuszewski, J., Nilges, M., Pannu, N. S., Read, R. J., Rice, L. M., Simonson, T., and Warren, G. L. (1998) *Acta Crystallogr. D54*, 905−921.
27. Jones, T. A. (1985) *Methods Enzymol. B115*, 157−171.
28. Laskowski, R. A., MacArthur, M. W., and Thorton, J. M. (1993) *J. Appl. Cryst. 26*, 283−291.
29. Frisch, M. J., Trucks, G. W., Schlegel, H. B., Scuseria, G. E., Robb, M. A., Cheeseman, J. R., Zakrzewski, V. G., Montgomery, J. A., Stratman, R. E., Burant, J. C., Dapprich, S., Millam, J. M., Daniels, A. D., Kudin, K. N., Strain, M. C., Farakas, O., Tomasi, J., Barone, V., Cossi, M., Cammi, R., Mennucci, B., Pomelli, C., Adamo, C., Clifford, S., Ochterski, J., Petersson, G. A., Ayala, P. Y., Cui Q., Morokuma, K., Malick, D. K., Rabuck, A. D., Raghavachari, K., Foresman, J. B., Cioslowski, J., Ortiz, J. V., Stefanov, B. B., Liu, G., Liashenko, A., Piskorz, P., Komaromi, I., Gomperts, R., Martin, R. L., Fox, D. J., Keith, T., Al-Laham, M. A., Peng, C. Y., Nanayakkara, A., Gonzalez, C., Callacombe, M., Gill, P. M. W., Johnson, B. G., Chen, W., Wong, M. W.,

Andres, J. L., Head-Gordon, M., Replogle, E. S., and Pople, J. A. (1998) *Gaussian 98*, revision A.6., Gaussian, Inc., Pittsburgh, PA.
30. Flükiger, P., Lüthi, H. P., Portmann, S., and Weber, J. (2000) *MOLEKEL 4.0*, Swiss Center for Scientific Computing, Manno (Switzerland).
31. Bzowska, A., Kulikowska, E., and Shugar, D. (2000) *Pharmacol. Therapeut. 88*, 349−425.
32. Berti, P. J., and Tanaka, K. S. E. (2002) *Adv. Phys. Org. Chem. 37*, 239−314.
33. Sauve, A. A., Cahill, S. M., Zeck, S. G., Evans, G. B., Furneaux, R. H., Tyler, P. C., Basso, L. S., Santos, D. S., Grubmeyer, C., Lewandowicz, A., McDermott, A. E., Girvin, M. E., and Schramm, V. L. (2003) *Biochemistry 42*, in press.
34. Kicska, G. A., Tyler, P. C., Evans, G. B., Furneaux, R. H., Shi, W., Fedorov, A., Lewandowicz, A., Cahill, S. M., Almo, S. C., and Schramm, V. L. (2002) *Biochemistry 41*, 14489−14498.
35. Mao, C., Cook, W. J., Zhou, M., Federov, A. A., Almo, S. C., and Ealick, S. E. (1998) *Biochemistry 37*, 7135−7146.
36. Hyland, L. J., Tomaszek, T. A., Jr., and Meek, T. D. (1991) *Biochemistry 30*, 8454−8463.
37. Ikeda, S., Ashley, J. A., Wirsching, P., and Janda, K. D. (1992) *J. Am. Chem. Soc. 114*, 7604−7606.

BI0343830